Wet foam flow: A suitable method for improving surface hygiene in the food industry

Heni Dallagi, Christine Faille, Laurent Bouvier, Maureen Deleplace, Thomas Dubois, Fethi Aloui, Thierry Benezech

Wet foam flow: a suitable method for improving surface hygiene in the food industry

Heni DALLAGI[a], Christine FAILLE[a], Laurent BOUVIER[a], Maureen DELEPLACE[a], Thomas DUBOIS[a], Fethi ALOUI[b], Thierry BENEZECH[a]*

[a] Univ. Lille, CNRS, INRAE, Centrale Lille, UMET, F-59000 Lille, France

[b] Polytechnic University Hauts-de-France, LAMIH CNRS UMR 8201, Campus Mont-Houy, F-59313 Valenciennes, France

***Corresponding Author:** Thierry BENEZECH, INRAE, UMET, 369 rue Jules Guesde, F-59650 Villeneuve d'Ascq, France. thierry.benezech@inrae.fr

ABSTRACT

In the food industry, the cleaning of contaminated surfaces requires new strategies to be adopted which can provide greater cleaning efficiency with minimal energy and water consumption. The use of wet foams was proposed to clean stainless steel surfaces contaminated by droplets containing *Bacillus* spores. Methods such as polarography, conductimetry and foam structure identification were used. Foam flow conditions with varying wall shear stresses and bubble sizes were observed to measure their impacts on surface contaminant removal kinetics. Compared to conventional cleaning-in-place method, foam flow more effectively removed both hydrophilic and hydrophobic spores. The combination of high shear stress and small bubble sizes (<0.2 mm) showed promise for improving the cleaning efficiency of the foam. Mechanisms such as fluctuation in local stresses, or in the liquid film thickness between the bubbles and the steel wall induced by bubble passage, foam imbibition and liquid film drainage were then investigated.

Keywords

Flow foam cleaning in place; *Bacillus* spores; conductimetry; polarography; bubble size; wall shear stress

1. Introduction

In the agro-food industrial environment, avoiding surface contamination by unwanted microorganisms is of crucial importance (Alvarez-Ordonez et al., 2019; Farag et al., 2021). Indeed, contaminated surfaces can recontaminate food in contact (cross-contamination), with sometimes disastrous consequences in terms of food spoilage, but also in terms of transmission of pathogens that can be the cause of large-scale epidemics. For example, surface contamination with microorganisms would have accounted for more than 50% of the collective foodborne illnesses (CFTI) in France between 2006 and 2008 (Delmas et al., 2010). Nowadays, cleaning-in-place (CIP) is a routine method in the food and pharmaceutical industries to ensure the equipment hygiene and the quality of product. The effect of the hydrodynamics of the cleaning fluid on CIP efficiency has been the subject of numerous studies (Li et al., 2019; Piepiórka-Stepuk et al., 2021). Particular interest has been shown in parameters such as the mechanical action exerted by the flow in creating wall shear stress (Bénézech and Faille, 2018) or the impact of Reynolds number (Fan et al., 2018). Their results showed that turbulence affects the cleaning process, as an increase in the presence of turbulent structures generated at the walls could improve the cleaning efficiency, but up to a certain limit. The use of non-stationary flows, such as pulsed flows and intermittent jet flows, would appear to increase CIP efficiency. Indeed, these kinds of flows affect both the mean and fluctuating components of the wall shear stress and consequently reduce the residual contamination (Absi and Azouani, 2018; Blel et al., 2013).

Gas-liquid two-phase flows (air bubbles in liquid or foam), which are also non-stationary flows, are likely to be of similar interest to pulsed flows. Indeed, liquid containing gas bubbles (non-foaming solution) had been shown to efficiently remove from surfaces both particles (Kondjoyan et al., 2009) and bacteria (Kriegel and Ducker, 2019). Recently, the efficiency of foam flow to remove *Bacillus* spores from stainless steel surfaces has been investigated by (Al Saabi et al., 2021) and the use of

aqueous unstable foams has also been proposed for cleaning the sensitive surfaces of artistic and cultural assets (Schad et al., 2021). It should also be noted that foam in static conditions, is widely used in the food industry for cleaning open surfaces (floors, conveyor belts, worktops and equipment) (Mierzejewska et al., 2014).

Aqueous foam could be considered as a non-Newtonian fluid consisting of gas dispersion in liquid containing surfactants. Depending mainly on the liquid fraction, the foam could be ranked as wet (small and spherical bubbles) or dry (large and polyhedral bubbles). A liquid-rich layer may be formed near a solid surface due to the bubble migration, thereby giving a slip effect between the foam and the wall (Tisné et al., 2003). Given this complexity, the rheological behavior of foam can follow the shear-thinning Herschel-Bulkley model, which states that under strong mechanical stresses, foam behaves as a viscous liquid, while under low stresses it behaves as a solid whose structure can be deformed and return to its initial state (Dallagi et al., 2019). Moreover, very wet foam flow (liquid fraction = 0.5) was found to clean hydrophilic spores better than dryer foam (liquid fraction between 0.3 to 0.4) (Al Saabi et al., 2021). However, the maximum of the shear stress that they used was 6 Pa, and the work lacks the explanation of the cleaning process.

The aim of this study was to investigate the potential role of the foam velocity and their structure (described by air/water content of the foam and size of air bubbles) in efficiently removing Bacillus subtilis spores. In this respect, different flow conditions of wet foam (liquid fraction = 0.5), by varying the shear stress (from 2 up to 13.2 Pa) and the foam structure, were carried out to test its efficiency. All cleaning conditions were tested on two *Bacillus* spore strains which differ only in their hydrophilic/hydrophobic character. Another originality of this present work is the detailed physical analysis of the dynamic behavior of foam and its structure and consequences at the wall to identify the underlying mechanisms of the bacterial spores' removal and choose the foam flow condition leading to optimal cleaning. The foam cleaning effectiveness was then compared to a standard CIP procedure.

2. Materials and Methods

2.1. Foam preparation

The foam production prototype was built according to a previous work (Al Saabi et al., 2021). The prototype is presented in Fig. 1. Briefly, foam was produced by pressurized air injection through a porous medium (pore sizes ranging from 1 to 1.6 µm) into an SDS surfactant (Sodium Dodecyl Sulfate (over 98.5% purity) dissolved in osmosed water (0.15% w/w) to avoid any unwanted interactions with ions contained in the standard tap water.

The physical properties of the foaming solutions used were a 1 Bar atmospheric pressure and 20°C standard temperature, a 997.9 kg/m^3 density (ρ_l), a 0.94 10^{-3} Pa.s dynamic viscosity (μ_l) and a 26.2 10^{-3} N/m surface tension (σ). The foam quality (β) describing the air/water content of the foam was calculated as follows (Equation 1) where Q_g and Q_l are respectively the gas and liquid flow rates.

$$\beta = \frac{Q_g}{Q_l + Q_g} \quad (1)$$

A foam quality of 0.5 was chosen in this work by varying the shear stress and the capillary forces. The capillary force of the bubble $F_c = \sigma 2\pi r$ is defined as the force due to surface tension that acts between the two halves of the bubble (Al-Qararah et al., 2013) with respect to the capillary pressure ($P_c = \frac{\sigma}{r}$) (Schad et al., 2021), where r is the bubble radius. The balance between the viscous drag forces versus surface tension forces of the foam can be represented by the non-dimensional capillary number $Ca = \frac{\mu_l v}{\sigma}$. μ_l and v are the dynamic viscosity of the liquid solution and the foam velocity, respectively.

Therefore, the first part presents a detailed characterization of these foam flow conditions in order to understand the mechanism by which the foam detached the spores, to identify the key parameters and then to test these new foam conditions on cleaning of stainless-steel coupons contaminated by *Bacillus* spores. Table 1 (in Result section) summarizes all the FFC conditions (quality of 0.5) and CIP. The foam mean velocity ($\bar{v}$) and the Reynolds number (Re) are determined from the following equations:

$$Re = \frac{\rho_f . \bar{v} . d_h}{\mu_f}$$ d_h being the hydraulic diameter (2)

$$\bar{v} = \frac{Q_l + Q_g}{S}$$ S being the duct section (3)

$$\rho_f = (1 - \beta) . \rho_l + \beta . \rho_g$$ ρ_l being the liquid density (4)

$$\mu_f = \frac{\mu_l}{1 - \mu_l{}^{1/3}}$$ (5)

The foam flow conditions varied from 1.5 to 13.5 cm/s (Q_g= Q_l; are 4.5, 9, 13.5, 27, and 40.5 l/h for the cases 1, 2, 3, 4, and 5 respectively). The three first cases correspond to the conditions used in a previous work (Al Saabi et al., 2021). Cases 4 and 5 have the highest velocities, which were generated using three parallel generators. CIP has the highest velocity, while the mean shear stress was similar to that in case 4.

2.2. Foam characterization

2.2.1. Foam morphology

Foam flow was visualized in order to observe the bubble's displacement at the channel walls, for a given interval. A Nikon D850camera, equipped with an AF-S Micro NIKKOR 60 mm f/2.8 G ED with a resolution of 8256 x 5504 pixels, was used to record foam microtexture and its associated bubble size distribution. For each foam flow condition, three images were captured then analyzed using Piximètre 5.1 R1540 software. First, the chosen images were calibrated, then were subjected to different image processing features (local threshold, filters…) to reduce the noise in order to better observe its contours. The bubble size distribution was then calculated according to usual granulometric distributions. To evaluate the heterogeneity/uniformity of this distribution, different parameters were identified such as *F0.05*, and *F0.2* corresponding to the percentage of the bubbles with a diameter of less than 0.05 and 0.2 mm respectively.

2.2.2. Thin film thickness

The conductimetry technique was used to measure the thickness of the thin film. This is based on the measurement of the impedance of the liquid volume located between the liquid-foam interface

and two outcropping electrodes at the duct wall. A generator provided an alternating sinusoidal voltage to power these electrodes. The frequency was 50 kHz to avoid any polarization phenomena. The calibration of the conductimetric probe was carried on using the calibrated Mylar sheets. The estimated error was 8%.

2.2.3. Wall shear stress

When foam flowed, mean shear stress was calculated based on the measurement of the static pressure along the channel. The power loss measurements were carried out using a differential pressure sensor Shlumberger, type 8D. Two pressure outlets allow the connection of 2 manifold tubes placed over a scaled plate that measures on a length L of 1m the pressure drop placed after 1.5 m from the entry of the foam in the duct. Indeed, to allow steady state flow conditions, the test ducts were placed at intervals exceeding 80 times the hydraulic diameter of the vein inlet (i.e. 1.5 m). The mean wall shear stress can thus be computed as:

$$\bar{\tau} = \frac{\Delta P}{\Delta x}\frac{d_h}{4} \quad (6)$$

where $\frac{\Delta P}{\Delta x}$ is the pressure gradient.

The local shear stress at the top wall where coupons were placed, was measured using the polarography method. This technique allows the determination of the local velocity gradient at the walls by measuring the mass transfer coefficient of the electrodes. Briefly, based on the simplified assumptions for the resolution of the convection-diffusion equation proposed by (Mitchell, 1965), the wall shear stress calculation was obtained from the velocity gradient (Lévêque solution and Sobolic correction). Details of the method used here were given previously (Tisné et al., 2003).

From a theoretical point of view, the polarographic signal is related to the slip layer thickness and foam velocities. The diffusion limit current can be represented as the Sherwood number form (*Sh*) or directly as the wall shear stress (τ_w). Spectral analysis of the time signals appears necessary in order to understand the underlying mechanisms and to trace back to the flow characteristics near the wall duct. The method used for spectral representation is based on the processing of the signal acquired by the Fourier transform (*FT*) with Matlab software. This was proposed by (Ioana et al., 2007). It

expresses the frequency distribution of the amplitude, the power spectral density, as well as the fluctuation rate of the considered signals. These specters revealed peaks obtained at characteristic frequencies corresponding to the passage frequencies of bubbles respective to each foam condition and their harmonics.

It was found that the SDS did not support the addition of electrochemical products (Ferri-ferrocyanide potassium) for the use of the polarography method. In fact, a reaction other than oxidation-reduction was produced, destabilizing the foam. For this reason, we replaced the SDS with a non-anionic surfactant: Lauramine oxides (Ammonyx® LO (Stephan) = 0.8 ml/l). To ensure the presence of the same phenomena for the same flow conditions, the thickness of the liquid film and of the conductivity signals produced with that of the SDS solution was verified. The same behavior and signal variation with SDS or Ammonyx® surfactant was observed, which is in line with previous works (Tisné et al., 2003), where another surfactant (Amonyl®) replaced the SDS for the same reason.

2.3. Bacterial strains and materials

Two *Bacillus subtilis* strains were used throughout this study. *Bacillus subtilis* PY79 (subsequently named Bs PY79) is a laboratory strain producing hydrophilic spores surrounded by a mucous layer called crust. A Bs PY79 recombinant strain deleted in *spsA* (Dubois et al., 2020), subsequently named Bs PY79 *spsA*, which produces hydrophobic spores modified in their crust properties, was also used throughout this study. Both *Bacillus* strains were tagged with green fluorescent proteins to make the spores more fluorescent. Spores were produced as previously described (Faille et al., 2019) on Spo8-agar at 30°C. When over 95% of spores were obtained, they were harvested by scraping the surface, washed five times in sterile water, and stored in sterile water at 4°C until use. In order to limit the presence of spore aggregates, the spore suspensions were subjected to an ultrasonication step (Bransonic 2510E-MT, Branson Ultrasonics Corporation, USA) before each experiment.

All experiments were carried out on AISI 316 stainless steel with pickled (2B) finish coupons (provided by APERAM, Isbergues, France) in the form of rectangular coupons (45 mm × 15 mm). In

196 order to have surface properties similar to those used in the dairy industry, the stainless-steel
197 coupons were subjected to a conditioning procedure consisting of 15 runs of soiling and cleaning
198 both to mimic what might occur in food processing lines and to stabilize their surface properties. The
199 soiling step was achieved by immersing the coupons in milk in semi-skimmed reconstituted milk (150
200 g/l milk powder) for 30 min at room temperature. After a quick rinse, soiled coupons were cleaned
201 by immersion in sodium hydroxide at 0.5% w/w for 30 min at 70°C. Before each experiment, coupons
202 were cleaned using an alkaline detergent (RBS T105, Traitements Chimiques des Surfaces, France).
203 Each coupon was first rubbed vigorously with pure RBS and then immersed for 10 minutes in 5% RBS
204 at 60°C. Coupons are thoroughly rinsed for 5 min with tap water, and then with softened (reverse
205 osmosis) water for another 5 min. One day before experiments, coupons were sterilized in a dry heat
206 oven at 180°C for 1h.
207 The hydrophilic character of the cleaned and disinfected coupons was estimated using a
208 goniometer (Digidrop, GBX, France). A water contact angle (θ_{water}) of 66° was measured, which
209 reflects the relatively hydrophilic character of this material.
210
211 **2.4. Surface soiling and cleaning**
212 For both strains, the concentration of the spore suspensions was set at 10^8 CFU/ml. Five 1 µl
213 droplets of the spore suspension were placed on each coupon and evaporated for 1h at 30°C. The
214 procedure was schematically illustrated Fig. S1. Some coupons were analyzed to control the initial
215 contamination level (5 10^5 spores per coupon) and to observe the droplet architecture under the
216 microscope (Fig. S1 in the Supporting Information). Then, sets of 4 coupons were placed inside a
217 rectangular stainless-steel duct (1.5 10^{-2}m high × 1 10^{-2}m width), subjected to a cleaning procedure
218 and analyzed again for residual contamination (three coupons) for enumeration and deposit
219 architecture (one coupon).
220 In this work, as previously (Al Saabi et al., 2021), the foam cleaning phenomenon was evaluated
221 at the top wall because the wall shear stress and the thin liquid film thickness would be considered to

show constant variations in this zone according to previous work (Tisné et al., 2004, 2003). This position was selected in order to facilitate the interpretation of the role of foam flow in the cleaning process.

The resistance of the spore deposits to a cleaning procedure was performed as follows. The test ducts were connected to the pilot rig and then were subjected to the cleaning process. Experiments were carried out on foam flow cleaning (FFC) under different conditions (by varying the foam shear stress and the foam/bubble structure) for 15 and 35 s, 1, 3, 5, 10, and 20 min. Other experiments were carried out on cleaning in place (CIP) under the same conditions to compare the relative effectiveness of FFC and CIP. Details are provided in the Results section. After the cleaning process, the coupons were removed from the test duct, then rinsed by immersion in sterile ultrapure water to remove the rest of the foam. In order to investigate the possible role of the presence of SDS surfactant on spore detachment, further experiments were performed in static conditions by dipping a set of coupons in pure water or in SDS 0.15% (w/w) for 20 min (data not shown). It should be noted that Bs spore incubation in SDS did not result in any significant viability loss.

To determine the quantity of spores on the coupons before and after cleaning, each coupon surface was sampled using a dry cotton swab (Copan, Brescia, Italy). The swabs were placed in a tube containing 5 ml of sterile ultrapure water and vortexed for 1 min at 2400 rpm. The suspensions containing the detached spores were enumerated on TSA (Tryptone Soy Agar, Biokar, France) after 48h at 30°C. For microstructure examination, the observation of some deposits was performed before and after cleaning, using an epifluorescence microscope (Zeiss Axioskop 2 Plus, Oberkochen, Germany). The observations were first made at low magnification (x50) in order to observe the whole deposit resulting from the drying of a droplet. Further observations were carried out at higher magnification (x400) to determine the fine structure of the densest parts of these deposits (clusters, peripheral rings…), including any 3D organization.

After cleaning, the deposits were mostly weakly fluorescent, which made them difficult to observe. It was therefore necessary to stain them before observation. For that purpose, dried coupons were stained with orange acridine (0.01%) for 15 min. In order to ensure that the deposits were not removed during this staining step, some deposits were observed before and after the staining step. No significant difference was observed.

2.5. Kinetics modeling

The removal kinetic profiles of the percentage of residual spores were fitted according to previous work (Bénézech and Faille, 2018), using GInaFIT. A two-phase model was selected (Equation 7), which presents the existence of two subpopulations characterized by different removal behaviors.

$$\frac{N}{N_0} = f\, e^{(-k_{max1}t)} + (1-f)e^{(-k_{max2}t)} \quad (7)$$

Where N_0 is the initial bacteria count, f is the poorly adherent fraction of the population (less resistant to detachment), ($1-f$) is the more adherent fraction, and k_{max1} and k_{max2} [s^{-1}] are the specific detachment rates of the two sub-populations.

2.6. Statistical analysis

All the experiments were carried out in triplicate. Statistical analyses were performed by general linear model procedures using SAS V8.0 software (SAS Institute, Gary, NC, USA). For each cleaning condition, variance analyses were performed to determine the possible role of the shear stress and the foam structure on the removal kinetics of spores (f, k_{max1}, and k_{max2}) and the effectiveness of the cleaning by foam flow compared to the CIP process.

3. Results

In this study on the detachment of adherent spores by foam, it was essential to dispose of a procedure allowing very reproducible contamination of the surfaces, both in terms of contamination

rates and in terms of the structure of the deposits. For this reason, we chose to contaminate the materials with droplets containing *Bacillus* spores and to let these deposits dry as previously described (Deleplace et al., 2021). For the type of foam (more or less dry), we chose to use a so-called wet foam (foam quality of 0.5) because recently published work had shown that dryer foams (liquid fraction from 0.4 to 0.3) were less effective (Al Saabi et al., 2021). We used SDS as model surfactant system to produce the foam. In order to identify the key parameters affecting the efficiency of foam cleaning, we first performed a series of physical measurements of foams obtained under different conditions, and we measured the effect of these parameters on the cleaning efficiency in terms of spores' detachment during cleaning procedure and patterns deposition after cleaning.

3.1. Foam flow characterization

3.1.1. Bubbles size distributions

Fig. 2 shows top views of the foam at the top wall for the different flow conditions. For all foam flow conditions, the bubbles had a roughly spherical shape and were separated by thick liquid films (lamellae). Different foam morphologies were observed. Indeed, when the velocity increased from 1.5 to 9 cm/s, a clear decrease in the bubble size was observed. However, no additional decrease could be observed between 9 and 13.5 cm/s. Bubble sizes were then measured for these different conditions and the curves of the cumulative fraction of the bubble size distributions are presented in Fig. 3. First, the distribution of the bubble size in all conditions was fitted by a lognormal function (R^2 ranging from 0.89 to 0.97) to better visualize the differences between the conditions tested. Variation of velocity causes a change in foam structure and bubble size distribution. As the foam velocity increased (Table 1), the mean diameter of bubbles decreased (from 0.34 down to 0.18 mm, for foam at 1.5 and 9 cm/s respectively) and the distribution became more homogeneous, except for foam at 13.5 cm/s where the mean diameter was 0.21 mm. While the number of small bubbles (less than 0.05 mm in diameter) was very close at 9 and 13.5 cm/s, intermediate-sized bubbles (between

0.2 and 0.6 mm in diameter) were more abundant at 9 cm/s than at 13.5 cm/s. Therefore, the cumulative bubble size number at 0.2 mm (*F02*) was 0.68 and 0.60 respectively for 9 and 13.5 cm/s, as indicated in Table 1 and were found to be statistically different ($Pr < 0.0001$). These differences were much greater when comparing the highest velocities to the lowest ones. Indeed, considering bubbles with a diameter ≤ 0.05 mm (see fraction *F005*, Table 1), at 13.5 cm/s the cumulative fraction was more than 20 times higher than that for the lowest foam velocities, at 1.5 cm/s.

3.1.2. Upper liquid film thickness

Foam is not in direct contact with the wall surface, but bubbles are slipping over a thin liquid film layer (a few micrometers width). Variations of the liquid film thickness (from 11 up to 13 µm) measured at the top wall are shown in Fig. 4 (left) for three foam mean velocities of 1.5, 3, and 4.5 cm/s, bearing in mind the limitations of our experimental set-up essentially due to the inability to access sufficiently high foam flow rates as it was possible for the cleaning experiments. The film thickness was affected by the bubble passage as shown in Fig. 4 (left) with an example of the observed temporal evolution of the signal at the middle of the test section. It should be noted that whatever the position of the probe the signal was observed as similar either on the sides or in the middle of the duct. In the three cases, conductimetry signals presented high fluctuations reflecting the non-uniformity of this liquid film. Indeed the signals showed an instantaneous variation of 72 and 54% relative to the mean thickness value which varied from 5 to 21 µm, and from 8 to 22 µm for foam at 1.5 and 4.5 cm/s, respectively. In addition, the profiles obtained appeared to be very different within the three cases. The higher is the velocity the higher is the frequency of the signal (variation from 45 to 72.5 Hz for cases of foam at 1.5 and 4.5 cm/s, respectively), and the lower is the amplitude (variation from 9.8 up to 6 µm, respectively). These variations were directly linked to the frequency of passage of the bubbles and to the size variations leading to the shape of the signal. Indeed, the maximum thickness of the liquid film (peaks of the signal) corresponds to the film thickness between two following bubbles passage, minimum thickness (signal hollows) corresponding to the presence of the bubble, the bigger bubble the lower film thickness could be

stated from Fig. 2. It should be noted that conductimetry results, for both tested surfactants SDS and Ammonyx, have shown the same instantaneous evolution and presented the same phenomena at the walls. A variation of 61 and 42% relative to the mean thickness and an increase of frequency from 37.5 to 77.5 Hz for cases of foam at 1.5 and 4.5 cm/s respectively, are shown in Fig. S2 in the Supporting Information.

3.1.3. Wall shear stress

To highlight the effect of the passage of a bubble on the shear rate at the wall, temporal signals from the frequency response of the polarography probe located in the middle of the channel have been plotted (Fig. 4, right).

The wall shear stresses on the upper region of the duct appeared larger and approximately double the value of the average stress measured on the section (data not shown). This is in relation to the low thickness of the liquid film at this location. The average shear stress increases slower than the foam flow velocity but increases from 4.3 Pa at 1.5 cm/s to 7.2 and 8.1 Pa for velocities of 3 and 4.5 cm/s, respectively. More interesting were the temporal variations of the wall shear stress at the top wall as shown in Fig. 4 (right), the signal varies periodically with a more homogeneous pattern with velocity increase but a decrease in amplitude is clearly visible at 4.5 cm/s. The rate of fluctuation of the wall shear (*RFS*) related to the signal amplitude decreases as the foam velocity increases reaching 957, 688, and 491% for the three foam velocities tested, 1.5, 3, and 4.5 cm/s respectively. The passage of bubbles, as seen in the film thickness variations, causes these variations in local shear stress. These fluctuations are therefore characterized by a frequency that corresponds directly to the frequency of bubble sliding on the upper wall.

Observing the spectral densities of the wall velocity gradient, all the curves had almost the same shape of which spectrums obtained with the probes gave a low energy level (Fig. S3 in the Supporting Information). The frequencies of bubbles are 20, 39, and 45 Hz for the first three cases respectively. For the other foam conditions, the frequency and the *RFS* were determined by the extrapolation of these experimental results and the theoretical correlations between the frequency and foam

parameters (where $f_{bi} = \frac{\beta.v}{d_{bi}}$, $A_{bi} = \frac{v}{f_{bi}}$, and d_{bi} are the frequency, amplitude, and diameter of i bubble). As was expected, foam at higher velocities (9 and 13.5 cm/s) had the highest frequency (76 Hz) with a strong decrease in the wall shear fluctuation rate (130% for foam at 9 cm/s) (Table 1). All results are reported in Table 1.

3.2. Spores' detachment

3.2.1. Resistance to cleaning procedures

The cleaning kinetics for the two bacterial spores are presented in Fig. 5 based on the evolution of the mean values of the logarithmic reduction of adherent spores with the cleaning time. In all cases, the detachment curves clearly showed two distinct phases. Both phases appeared to be exponential and therefore were quite accurately described by the biphasic model, with R^2 ranging from 0.84 to 0.97. Whatever the flow conditions, the first detachment phase lasted less than 1 min, and the duration of this phase depended on the flow conditions of the foam (shorter at low velocity, for the two spores), but especially on the strain. At 1 min, the resulting log reduction of the adherent spores during this first phase ranged between 1.94 and 2.6, and between 0.95 and 1.33 for Bs PY79 and Bs PY79 *spsA*, respectively. The second phase was much longer and would probably continue over 20 min. The detachment rate of the hydrophilic spores (Bs PY79) during this second phase was quite low at 1.5, 4.5, and 13.5 cm/s resulting in an additional 0.15-0.28 log reduction of the adherent spores, whereas at 9 cm/s the reduction reached around 1.15 log. A similar trend was observed for the hydrophobic spores with 0.2-0.3 log reduction at 1.5, 4.5, and 13.5 cm/s and 0.45-0.57 log reduction at 9, and 13.5 cm/s.

The role of the flow parameters and strains on the three kinetics parameters (f, k_{max1}, and k_{max2}) was then investigated. When comparing the two strains, the influence of the strains on the removal efficiency during the first phase represented by the two parameters f (poorly adherent fraction of the population) and k_{max1} (first kinetics constant rate) was highly significant as confirmed by the variance analysis ($Pr < 0.0001$ for both parameters). According to Tukey's groupings, f was significantly

377 affected by the strain, with mean values of 0.92 and 0.998 for Bs PY79 *spsA* and Bs PY79 respectively
378 as shown in Fig. 6. The initial detachment rate (k_{max1}) also was largely dependent on the strain (from
379 1.7 up to 3.4 times higher for hydrophilic spores), while the second detachment rate (k_{max2}) was not
380 affected and was quite similar for the two strains (Fig. 6, no significant differences).

381 The role of the flow parameters as the shear stress (mean value, frequency, and *RFS*) and/or to
382 the distribution of bubbles (mean diameter and *F02*) on the three kinetics parameters (f, k_{max1}, and
383 k_{max2}) was then investigated (Table 2 and Fig. 7). Whatever the parameter in relation to the flow and
384 the bubble size arrangement the Tukey's grouping tests gave the same ranking between the 4
385 velocities tested (Table 2) and can be visualized clearly in Fig. 7, the two groups of parameters as the
386 ones related to the wall shear stress and the ones related to the bubbles' size influencing, in the
387 same way, the removal kinetics. However, differences between the two strains could be stated. For
388 Bs PY79, the first kinetics phase rate constant k_{max1} was similar for all the studied cases (no difference
389 according to the Tukey' test) but an effect was observed on f with a significant difference between
390 the lowest and the highest velocities (1.5 and 4.5 compared to 9 and 13.5 cm/s) leading however to
391 an improvement while increasing the mean shear stress (Fig. 7, black dots). Conversely, k_{max2} was
392 significantly higher in the case of foam at 9 cm/s comparatively to the other cases whatever the
393 strains. Some differences could be seen with the hydrophilic spores, according to Tukey's grouping in
394 Table 2 and Fig. 7, red dots. Indeed, the maximum foam velocity tested induced a significantly
395 higher value of f ($Pr < 0.0001$), a phenomenon more marked than with hydrophilic spores, as for
396 k_{max1}, it was significantly higher at this velocity than at the lowest velocity tested ($Pr < 0.013$).
397 However, k_{max2} variation trend with the velocity was similar to those of the hydrophilic strain and also
398 highly significant ($Pr < 0.0007$), the velocity of 9 cm/s being the best option. It should be noted that it
399 was not the highest mean shear stress tested (13.2 Pa), but it has the lowest bubble sizes (mean
400 diameter of 0.18 mm and *F02* of 0.68).

401 Cleaning with foam was then compared to a CIP procedure (pink and black curves in Fig. 5) using
402 the SDS solution at a shear stress of 9.8 Pa, shown to be the most efficient condition with foam.

Concerning hydrophilic spores, the first detachment's phase in the case of CIP was shorter than for foam cleaning and the removal was 0.5 log CFU less efficient. In addition, very few spores were detached in the second phase, resulting in about 2 log CFU reduction after 20 min cleaning compared to around 4 log CFU with foam. The same trend was observed with hydrophobic spores but at a lesser extent, the use of foam allowing an improvement in detachment efficiency of only 0.5 log in 20 min compared to CIP. The variance analysis confirmed that whatever the strains significant differences could be observed between CIP and FFC considering the two kinetics parameters f and k_{max2} ($Pr < 0.034$ and less than 0.001 respectively), k_{max1} being apparently not significantly modified (Fig. S4 in the Supporting Information).

3.2.2. Deposition patterns before and after cleaning

In order to observe whether the different areas of the dried drops were more or less easily removed during the cleaning procedures, the dried deposits were observed before cleaning and after 15 seconds and 20 minutes of cleaning. Two different deposition patterns were observed in epifluorescence microscopy (Fig. S4 in the Supporting Information). Whatever the spores, a regular round peripheral ring, often referred to as the "coffee ring" was clearly observed. For Bs PY79 spores, this external coffee ring shape was thick with relatively few adhered spores within the ring. Depending on the trial, the internal deposition was more or less regular, as if the contact line remained fixed or detached and then reattached, resulting in one or more small contaminated areas. Conversely, with the hydrophobic spores Bs PY79 *spsA*, a diffuse peripheral deposit was often observed, within which single spores but also spore clusters are present over the whole surface.

After cleaning, the observation of the residual patterns shown a good agreement with the enumeration results (Fig. 8). First, Bs PY79 spores seemed to be removed in a higher extent compared to Bs PY79 *spsA* spores. In the case of Bs PY79 spores after 15 s, the peripheral ring was partially removed by the cleaning procedure and this was particularly noticeable at 13.5 cm/s, but especially at 9 cm/s. After 20 min of cleaning, the ring had completely disappeared at 9 and 13.5 cm/s and to a lesser extent at 4.5 cm/s. However, spores were still visible on the inner area of the

deposits except for foam after 20 min at 9 cm/s. Regarding the cleaning of Bs PY79 *spsA* spores, spores, and small clusters seemed to be greatly removed while the larger clusters seemed to have better resisted the detachment, and the peripheral ring was partially removed only after 20 min. For both strains, removal was visibly greater with foam flow at 9 cm/s than CIP. At 15 seconds, the cleaning of the deposits of hydrophobic spores Bs PY79 *spsA* seemed to induce a slid of the contamination along the surface in the direction of the flow showing a quite scattered pattern visible with foam flow cleaning and CIP (blue arrows on Fig 8). This sliding phenomenon was absent in the case of hydrophilic spores Bs PY79.

4. Discussion

Foam has been considered as a non-Newtonian fluid and the Herschel–Bulkley model can predict its flow behavior as previously described (Dallagi et al., 2019). At low shear stress (2.2 Pa) the foam flow behaved as a plug flow in one direction, the velocity of the foam being uniform over the entire section as a 1-Dimensional (1D) flow regime. When the wall shear stress exceeded 4.2 Pa the plug behavior remained only at the top side of the duct (2D flow regime), and at shear stresses greater or equal to 5.9 Pa, the foam became completely sheared (3D flow regime) (Al Saabi et al., 2021). The rheological behavior of foams is controlled by processes that occur within the microstructures such as the rearrangement of bubble size, liquid film, and Plateau borders. A slight modification on the pressure or the shear stress applied could lead to deformation on the foam state. In previous studies on the rheology of emulsion and foam, authors have demonstrated the deformation of the bubble as a function of the capillary number (Llewellin and Manga, 2005). Their results show that as the capillary number increases, bubbles start to deform and the film separating bubbles either thicken or shrink trends to maintain the minimal surface energy. However, this deformation can result in developing anisotropy in foams properties if the capillary number exceeds a critical value which is

not the case here: for all studied cases *Ca* was lower than 0.1 and the bubbles remained almost spherical with isotropy of the foam nearly preserved.

It should be noted that except for the three foam conditions at 1.5, 3, and 4.5 cm/s obtained using 1, 2, or 3 generators with the same surfactant, flow rate, and air pressure content, the increase of the foam velocity up to 9 and 13.5 cm/s was obtained by increasing the surfactant flow rate and air pressure and content in the foam generators. It was demonstrated that the pressure significantly affects the foam texture, and its stability with a potential change in bubble size distributions, liquid drainage, and bubble coalescence (Al-Qararah et al., 2013), a reduction in the average radius of bubbles was observed with the increase of the pressure. These authors reported that the bubble size decreases with the increasing of the rotation speed up to a certain limit under axial mixing in a Becher. At a rotation lower than 5500 RPM (revolution per minute), the foam remains stable since the air is well homogenized in the surfactant solution. Conversely, above 5500 RPM, because of the saturation of air content, the interactions between bubbles were more numerous which favored their coalescence. Thus, their size increases, resulting in a decrease in interfacial stability. The observation of the foam at the highest velocity (13.5 cm/s) allowed to suggest that the large bubbles are more likely the consequence of a movement inside the foam (3D flow regime) allowing the larger bubbles indeed less dense to rise towards the upper wall rather than a coalescence of the bubbles explained by the high speed of the foam. This behavior was probably enhanced by the fact that the foam is quite wet with a quality β of 0.5.

Furthermore, the conductimetry and polarography results (Fig. 4) demonstrated a significant impact of the velocity of the bubbles and their sizes on the fluctuation of the liquid film thickness between bubbles and the top wall and on the local wall shear stress increases significantly between two consecutive bubbles (Plateau borders). These variations would directly affect bacteria present at the surface influencing the removal phenomenon. The displacement of the bubbles leads to sudden increases in the Sherwood number due to shear stress peaks, appearing in a harmonic manner directly related to the bubble passage frequency. Comparing foams at 1.5, 3, and 4.5 cm/s, as the

480 velocity increased, the bubbles became smaller with an F02 of 0.29, 0.36, and 0.44. The frequency of
481 the shear stress increased in parallel from 20 up to 45 Hz while amplitude decreased in agreement
482 with previous works (Tisné et al., 2003). Hence, foam at 9 cm/s having a higher amount of small
483 bubble sizes presented the lowest *RFS* (*RFS* of 130 %) with the high frequency (*f* of 70 Hz) related to
484 the thin liquid film height variation measurements. The peaks of the shear stress were clearly
485 observed at the two ends of the bubbles, the bubble front, and the back. As an example, the wall
486 shear stress value between the bubbles is about 15 Pa while it remains lower than 2 Pa under the
487 bubbles, for foam at 4.5 cm/s. These values corresponded therefore to the maximum and minimum
488 film thickness observed, respectively. In the literature, CFD simulations, as well as experimental
489 studies in two-phase gas-liquid slug flow, e.g. in capillary membranes (Kumari et al., 2018), suggested
490 that the major contribution to the wall shear stress came from the bubbles ends and could be
491 attributed to the Laplace pressure difference caused by the surface tension. (Tisné et al., 2004)
492 revealed that it was possible to relate foam flow study to studies of a long bubble moving in
493 capillaries, and they observed that the bubbles moved as flattened bubbles in a Hele-Shaw cell
494 confirming the localization of the shear stress on the Plateau borders.

495 When compared with spore removal kinetics, parameters in relation to the shear stress and
496 bubble size variations seemed to play a significant role in the cleaning efficiency of foam flow. For
497 both Bs strains, the increase of the mean shear stress roughly leads to an improvement in the
498 cleaning efficiency. However, it was not true for the foam at 13.5 cm/s, which showed a reduction in
499 cleaning efficiency, compared to 9 cm/s. This result suggests that other parameters than the mean
500 shear stress were involved in the FFC efficiency and therefore the variation of the local wall shear
501 stress (WSS) as discussed above in relation to the size and the velocity of the bubbles could play a
502 major role. These results are consistent with previous works in literature. Silva et al. highlighted the
503 significant role of the WSS fluctuation on the cleaning efficiency using pulsed flow (Silva et al., 2021).
504 Results showed that shorter periods promoted higher removal of raw milk cells due to the
505 occurrence of the annular effect and its important frequency. A higher frequency of peaks WSS was

needed to make turbulent pulse flow effective to remove tomato deposits (Absi and Azouani, 2018). The authors explained obtained results by the fact that at higher frequency the surfaces are submitted more often to the phenomenon caused by peaks. Hence, as the foam has a higher amount of small bubbles, the contamination will be more subjected to the pick of WSS and perhaps also to the viscous dissipation in the narrow Plateau borders between consecutive bubbles since smaller bubbles possess a higher Laplace pressure.

Whatever the FFC conditions, the removal kinetics showed a strong detachment rate at the beginning of the cleaning process (less than 1 min), followed by a second kinetic phase described by a slow detachment rate. Previous works on biofilm removal under CIP (Bénézech and Faille, 2018) and bacteria spores under different foam qualities (Al Saabi et al., 2021) have reported similar observations. Neither the shear stress nor the bubble size has affected the first kinetic phase rate of removal with Bs PY79 spores, while high shear stress induced low k_{max1} with Bs PY79 *spsA*. For both strains, as the shear stress increased, the f parameter increased (the spore population detached more easily). The synergy between high shear stress and small bubbles (foam at 9 cm/s) would explain the highest k_{max2} and a better cleaning efficiency. To prove or disprove this suggestion, a new foam flow condition was produced at 9 cm/s, using a single generator. The air pressure in the generator in this condition was 3 times more than that for the 9 cm/s foam, produced by three parallel generators. As was expected, the mean shear stress was 9.8 Pa, while the bubble size increased (mean diameter of 0.19 mm with a presence of large bubbles (Fig. S5 in the Supporting Information). When comparing the second detachment phases, foam with the smallest bubbles was more efficient for PY79 spores, by 1 log CFU over 20 min. k_{max2} was 1.5 times higher (with 9.8 Pa foam and small bubble size) than that in the alternative condition tested. For *spsA* spores, k_{max2} seems to be similar in these two conditions.

According to (Kondjoyan et al., 2009), the role of capillary forces is not negligible and depends on the size of the bubbles and their speed. In (Al Saabi et al., 2021), the detachment of the hydrophilic spores of *Bacillus amyloliquefaciens* 98/7 occurred at bubble velocities of around 3 cm/s and

dramatically decreased at 5 cm/s in line with the work of (Kondjoyan et al., 2009), where the greatest detachment rate was observed, as illustrated by high k_{max1} constant rate values. In this work, no visible changes could be seen for the first kinetic phase with the increase in the foam velocity from 9.5 up to 13.5 cm/s, but the second kinetic phase showed a significant decrease in the removal efficiency. For hydrophobic particles, according to (Kondjoyan et al., 2009), the detachment rate would start at higher bubble velocities. In this work, the increase in the foam velocity indeed was accompanied by an increase in the detachment efficiency during the first minutes of the foam cleaning, which corresponds to an increase in the *f* parameter, resulting in a more rapid and efficient spore removal.

Other phenomena would occur under the combination of the drainage and the imbibition effects (Fig. 9). It is known that under gravity and capillarity, the liquid flows through drainage networks called Plateau borders. This phenomenon has been demonstrated in previous works (Maestro et al., 2013). Thus, as discussed before, the spores present in the thin liquid film between the bubble and the solid surface are prone to be absorbed within the Plateau borders under the imbibition effect. This mechanism is driven by the capillary forces. Indeed, these Plateau borders have a curvature that creates a capillary under-pressure in the liquid phase. Owing to this pressure difference, the foam was able to absorb the spores (which were in small size,1 µm), just as a sponge would. It has been proven in the literature that the imbibition mechanism was highly dependent on the bubble size, which is the strongest for foam with a smaller bubble size (Maestro et al., 2013; Mensire et al., 2015). On the other hand, such a mechanism could help in understanding the difference in the results obtained by the two strains of spores. Unlike hydrophilic spores which can be easily trapped by the liquid film, absorbed into the Plateau border and then flushed out of the duct, the hydrophobic character of Bs PY79 *spsA* gives spores a strength to oppose the imbibition effect. They mostly remain in the liquid film and then due to bubble fluctuations, some of them are able to re-adhere to the solid surface. To highlight this phenomenon, the ability of hydrophobic spores to adhere to sterile coupons was tested at a distance of around 10 cm downstream of the contaminated area.

Whatever the flow conditions, results showed that 1.3% of the detached hydrophobic spores after 20 min of cleaning were able to re-adhere to the surface. Comparatively, the re-adhesion of hydrophilic spores was found to be negligible, at less than 0.1% of the detached spores after 20 min. Otherwise, due to the continuous fluctuations of the shear stress and the liquid film thickness induced by the bubble passage, some spores that were strongly attached to the surface were pushed to other locations, thereby causing a sliding phenomenon. This phenomenon was more visible in the case of hydrophobic spores than for hydrophilic ones. This could be explained by the strongly hydrophobic character of Bs PY79 *spsA*. Recently, Schad et al. have shown that foams with small bubble sizes are more efficient in cleaning glass surfaces contaminated with fluorescent oil (Schad et al., 2021). The authors explained the cleaning by an interplay of imbibition, drainage, and wiping mechanisms. Imbibition and drainage of oil into the Plateau borders of foams were found to be the strongest with small bubbles, which is in concordance with our results. However, the wiping mechanism, i.e., shifting of the contact line between foam, oil and glass was found to be more efficient with unstable foam than with a stable one. This is not surprising since they used static foam. Given similar conditions, unstable foams clearly clean better than stable foams, being continuously in motion and accelerating the re-arrangements of their bubbles with time which leads, as they explained, to violent wiping motions between the foams and the interface. Consequently, these are not completely irrelevant with our work since in our study foams were used in a dynamic form and the movement/flow was imposed, leading to forceful wiping. However, the instability of foam can reduce the cleaning efficiency through the generation of large bubbles (as observed in the case of foam at 9 cm/s).

5. Conclusion

In this study, we analysed the ability of wet foam flow to remove *Bacillus subtilis* spores from dried droplets on stainless steel surfaces. Two strains, *Bs* PY79 and *Bs* PY79 *spsA*, of different

hydrophobicity were used. Regardless of the strain, the foam flow showed a better removal capacity than conventional cleaning in place at the same average shear stress. Optimisation and improvement of cleaning efficiency using foam flow requires a quantification of the key parameters, such as bubble size, liquid film thickness and wall shear stress. Analyses obtained from polarography, conductimetry and bubble size quantification have shown that the magnitude and frequency of fluctuations in wall shear stress and liquid film thickness are related to bubble size and flow velocity. These phenomena are most likely to be the cause of spore removal, as described in the literature, although to a lesser extent, for cleaning with liquid solutions. In contrast, with foam, the particularity of fluctuations at the wall (liquid film thickness and shear stress) in relation to the bubble sizes and their velocities, combined with other probable phenomena such as imbibition and drainage of the liquid film within the foam, favours not only the release of contaminants, but also their entrapment. This leads to the conclusion that a combination of high WSS, and the presence of small bubbles (<0.2 mm) indeed improves surface biocontamination cleaning efficiency. Further studies would be interesting to test the ability of this process to clean actual industrial equipment, which is frequently of complex design. Further research could also be carried out into the removal of other types of microbial fouling by these flowing foams, such as into biofilm contaminations developed on the surfaces of materials other than steel, such as polymers, which are sometimes rougher and often more hydrophobic. The implementation of such a foam cleaning technology for CIP cleaning would request an effective foam removal during the rinsing step. Future work could be envisaged to solve this problem using stimuli-responsive surfactants allowing at request a complete disappearance of the foam.

Acknowledgments

The authors are grateful to Christelle Lemy and Laurent Wauquier from UMET, for their valuable technical assistance.

Funding

610 This work was supported by the region Hauts-de-France through their funding of the Interreg Veg-I-
611 Tec project (Programme Interreg V France-Wallonia-Flanders, GoToS3) and the ANR (Agence
612 Nationale de la Recherche) for funding of the FEFS project (contract number ANR-18-CE21-0010).
613
614

615 **References**

616 Absi, R., Azouani, R., 2018. Toward automatic cleaning of industrial equipment: pulsed flow-induced
617 wall shear stress. Procedia CIRP 78, 359–363. https://doi.org/10.1016/j.procir.2018.10.001
618 Al Saabi, A., Dallagi, H., Aloui, F., Faille, C., Rauwel, G., Wauquier, L., Bouvier, L., Bénézech, T., 2021.
619 Removal of Bacillus spores from stainless steel pipes by flow foam: Effect of the foam quality
620 and velocity. Journal of Food Engineering 289, 110273.
621 https://doi.org/10.1016/j.jfoodeng.2020.110273
622 Al-Qararah, A.M., Hjelt, T., Koponen, A., Harlin, A., Ketoja, J.A., 2013. Bubble size and air content of
623 wet fibre foams in axial mixing with macro-instabilities. Colloids and Surfaces A:
624 Physicochemical and Engineering Aspects 436, 1130–1139.
625 https://doi.org/10.1016/j.colsurfa.2013.08.051
626 Alvarez-Ordonez, A., Coughlan, L.M., Briandet, R., Cotter, P.D., 2019. Biofilms in Food Processing
627 Environments: Challenges and Opportunities. Annu. Rev. Food Sci. Technol. 10, 173–195.
628 https://doi.org/10.1146/annurev-food-032818-121805
629 Bénézech, T., Faille, C., 2018. Two-phase kinetics of biofilm removal during CIP. Respective roles of
630 mechanical and chemical effects on the detachment of single cells vs cell clusters from a
631 Pseudomonas fluorescens biofilm. Journal of Food Engineering 219, 121–128.
632 https://doi.org/10.1016/j.jfoodeng.2017.09.013
633 Blel, W., Legentilhomme, P., Bénézech, T., Fayolle, F., 2013. Cleanabilty study of a Scraped Surface
634 Heat Exchanger. Food and Bioproducts Processing 91, 95–102.
635 https://doi.org/10.1016/j.fbp.2012.10.002
636 Dallagi, H., Al Saabi, A., Faille, C., Benezech, T., Augustin, W., Aloui, F., 2019. CFD Simulations of the
637 Rheological Behavior of Aqueous Foam Flow Through a Half-Sudden Expansion, in: Volume 1:
638 Fluid Mechanics. Presented at the ASME-JSME-KSME 2019 8th Joint Fluids Engineering
639 Conference, American Society of Mechanical Engineers, San Francisco, California, USA, p.
640 V001T01A030. https://doi.org/10.1115/AJKFluids2019-4650
641 Deleplace, M., Dallagi, H., Dubois, T., Richard, E., Ipatova, A., Bénézech, T., Faille, C., 2021. Structure
642 of deposits formed by drying of droplets contaminated with Bacillus spores determines their
643 resistance to rinsing and cleaning. Journal of Food Engineering 110873.
644 https://doi.org/10.1016/j.jfoodeng.2021.110873
645 Delmas, G., Jourdan da Silva, N., Pihier, N., Weil, F.-X., Vaillant, V., De Valk, H., 2010. Les toxi-
646 infections alimentaires collectives en France entre 2006 et 2008 6.
647 Dubois, T., Krzewinski, F., Yamakawa, N., Lemy, C., Hamiot, A., Brunet, L., Lacoste, A.-S., Knirel, Y.,
648 Guerardel, Y., Faille, C., 2020. The sps Genes Encode an Original Legionaminic Acid Pathway
649 Required for Crust Assembly in Bacillus subtilis. mBio 11, e01153-20,
650 /mbio/11/4/mBio.01153-20.atom. https://doi.org/10.1128/mBio.01153-20
651 Faille, C., Lemy, C., Allion-Maurer, A., Zoueshtiagh, F., 2019. Evaluation of the hydrophobic properties
652 of latex microspheres and Bacillus spores. Influence of the particle size on the data obtained
653 by the MATH method (microbial adhesion to hydrocarbons). Colloids and Surfaces B:
654 Biointerfaces 182, 110398. https://doi.org/10.1016/j.colsurfb.2019.110398
655 Fan, M., Phinney, D.M., Heldman, D.R., 2018. The impact of clean-in-place parameters on rinse water
656 effectiveness and efficiency. Journal of Food Engineering 222, 276–283.
657 https://doi.org/10.1016/j.jfoodeng.2017.11.029
658 Farag, M.A., Mesak, M.A., Saied, D.B., Ezzelarab, N.M., 2021. Uncovering the dormant food hazards, a
659 review of foodborne microbial spores' detection and inactivation methods with emphasis on
660 their application in the food industry. Trends in Food Science & Technology 107, 252–267.
661 https://doi.org/10.1016/j.tifs.2020.10.037
662 Ioana, C., Mansour, A., Quinquis, A., Radoi, E., 2007. Le traitement du signal sous Matlab: Pratique et
663 applications, Hermes Science.
664 Kondjoyan, A., Dessaigne, S., Herry, J.-M., Bellon-Fontaine, M.-N., 2009. Capillary force required to
665 detach micron-sized particles from solid surfaces—Validation with bubbles circulating in

water and 2µm-diameter latex spheres. Colloids and Surfaces B: Biointerfaces 73, 276–283. https://doi.org/10.1016/j.colsurfb.2009.05.022
Kriegel, A.T., Ducker, W.A., 2019. Removal of Bacteria from Solids by Bubbles: Effect of Solid Wettability, Interaction Geometry, and Liquid–Vapor Interface Velocity. Langmuir 35, 12817–12830. https://doi.org/10.1021/acs.langmuir.9b01941
Kumari, S., Kumar, N., Gupta, R., 2018. Effect of gas–liquid ratio on the wall shear stress in slug flow in capillary membranes. Asia-Pac J Chem Eng 13, e2258. https://doi.org/10.1002/apj.2258
Li, G., Tang, L., Zhang, X., Dong, J., 2019. A review of factors affecting the efficiency of clean-in-place procedures in closed processing systems. Energy 178, 57–71. https://doi.org/10.1016/j.energy.2019.04.123
Llewellin, E.W., Manga, M., 2005. Bubble suspension rheology and implications for conduit flow. Journal of Volcanology and Geothermal Research 143, 205–217. https://doi.org/10.1016/j.jvolgeores.2004.09.018
Maestro, A., Drenckhan, W., Rio, E., Höhler, R., 2013. Liquid dispersions under gravity: volume fraction profile and osmotic pressure. Soft Matter 9, 2531. https://doi.org/10.1039/c2sm27668b
Mensire, R., Piroird, K., Lorenceau, E., 2015. Capillary imbibition of aqueous foams by miscible and nonmiscible liquids. Phys. Rev. E 92, 053014. https://doi.org/10.1103/PhysRevE.92.053014
Mierzejewska, S., Masłowska, S., Piepiórka-Stepuk, J., 2014. Evaluation of the efficiency of removing protein deposits from various surfaces by foam cleaning. Agricultural Engineering 131–137. https://doi.org/10.14654/ir.2014.149.014
Mitchell, J.E., 1965. Investigation of wall turbulence using a diffusion-controlled electrode. University of Illinois.
Piepiórka-Stepuk, J., Diakun, J., Sterczyńska, M., Kalak, T., Jakubowski, M., 2021. Mathematical modeling and analysis of the interaction of parameters in the clean-in-place procedure during the pre-rinsing stage. Journal of Cleaner Production 297, 126484. https://doi.org/10.1016/j.jclepro.2021.126484
Schad, T., Preisig, N., Blunk, D., Piening, H., Drenckhan, W., Stubenrauch, C., 2021. Less is more: Unstable foams clean better than stable foams. Journal of Colloid and Interface Science 590, 311–320. https://doi.org/10.1016/j.jcis.2021.01.048
Silva, L.D., Filho, U.C., Naves, E.A.A., Gedraite, R., 2021. Pulsed flow in clean-in-place sanitization to improve hygiene and energy savings in dairy industry. J Food Process Eng 44. https://doi.org/10.1111/jfpe.13590
Tisné, P., Aloui, F., Doubliez, L., 2003. Analysis of wall shear stress in wet foam flows using the electrochemical method. International Journal of Multiphase Flow 29, 841–854. https://doi.org/10.1016/S0301-9322(03)00038-7
Tisné, P., Doubliez, L., Aloui, F., 2004. Determination of the slip layer thickness for a wet foam flow. Colloids and Surfaces A: Physicochemical and Engineering Aspects 246, 21–29. https://doi.org/10.1016/j.colsurfa.2004.07.014

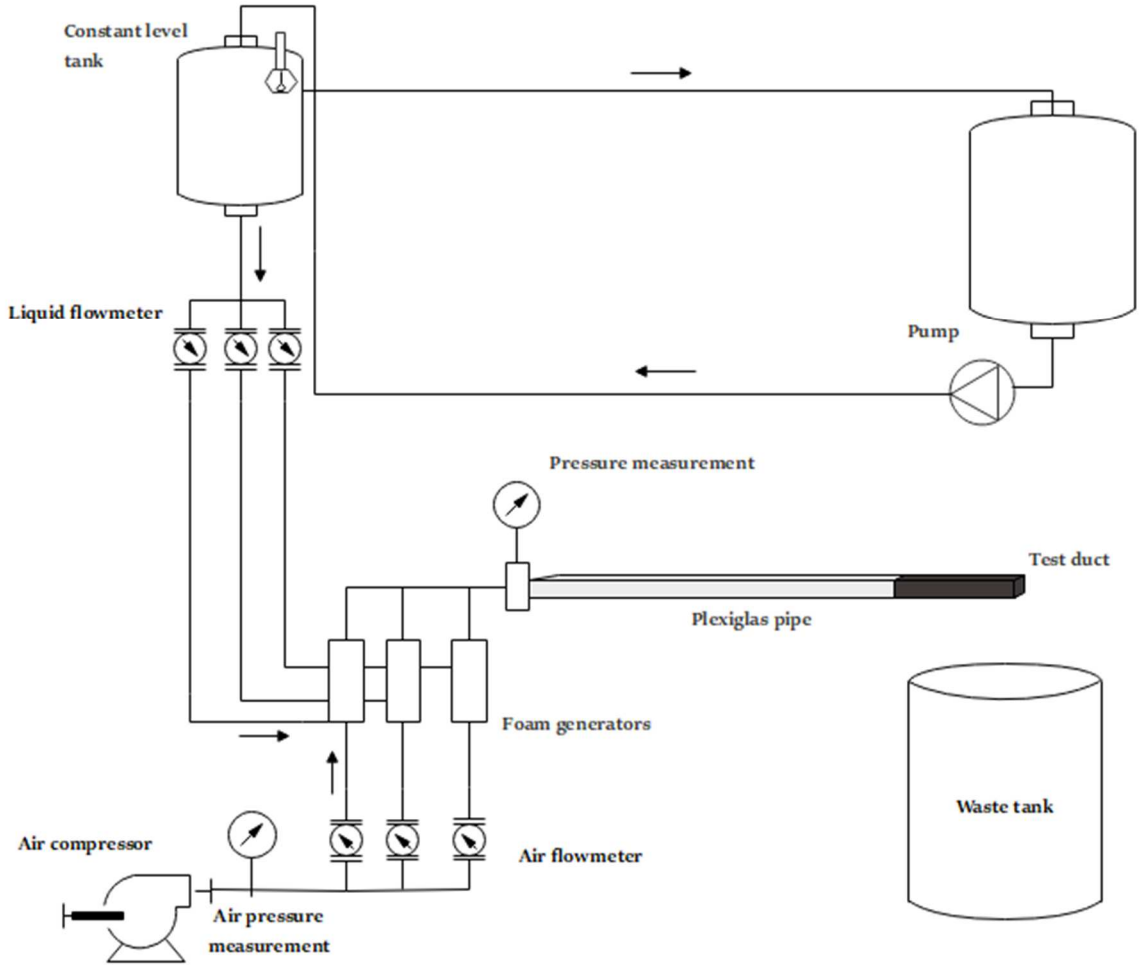

Fig. 1. Experimental set-up for studying the foam cleaning in place process.

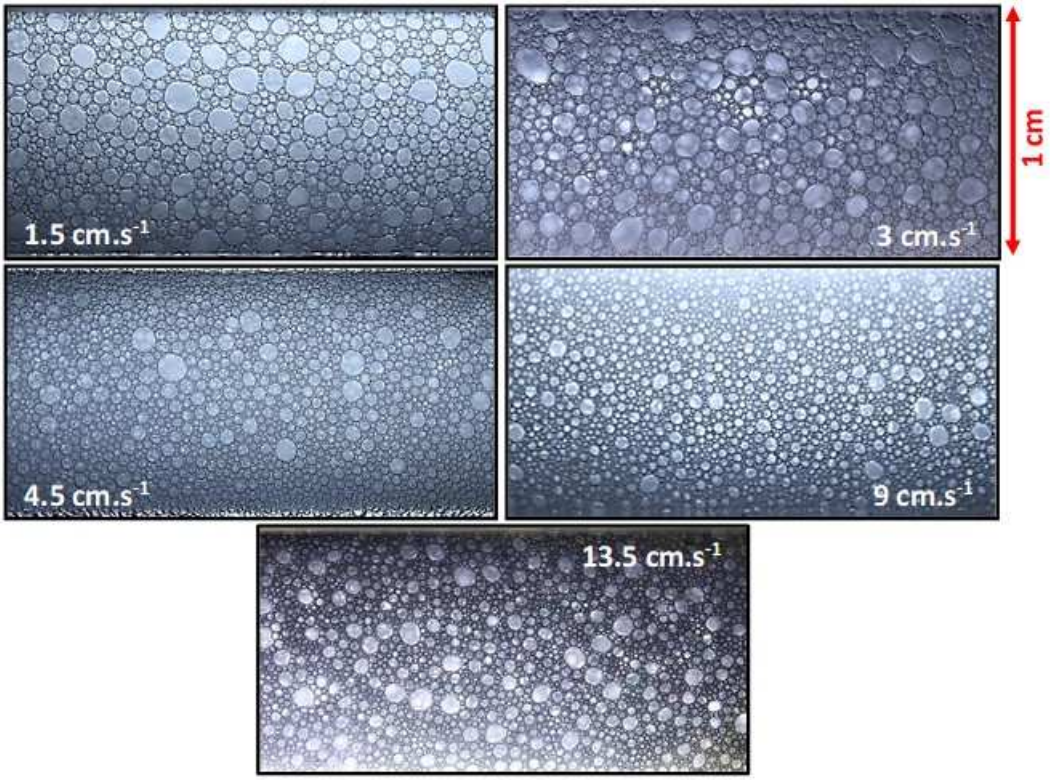

Fig. 2. Top view of foam at the wall of the transparent pipe (the entire width, 1 cm) for the different foam flow conditions.

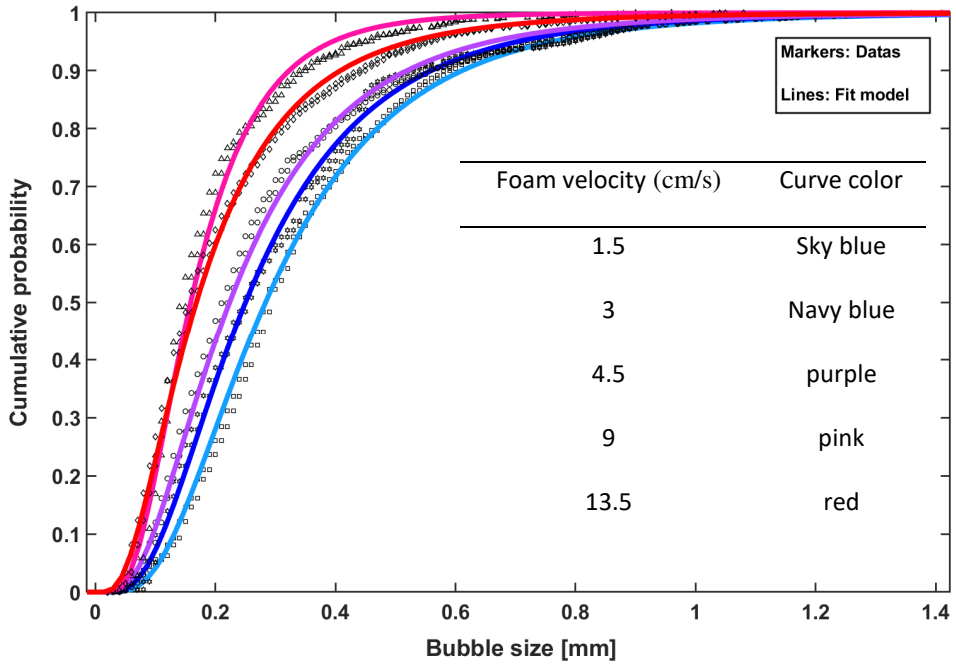

Fig. 3. Cumulative fraction of the bubble size distribution for all the foam flow conditions. The markers present the brut data and the lines represent the Lognormal model fitted to each condition.

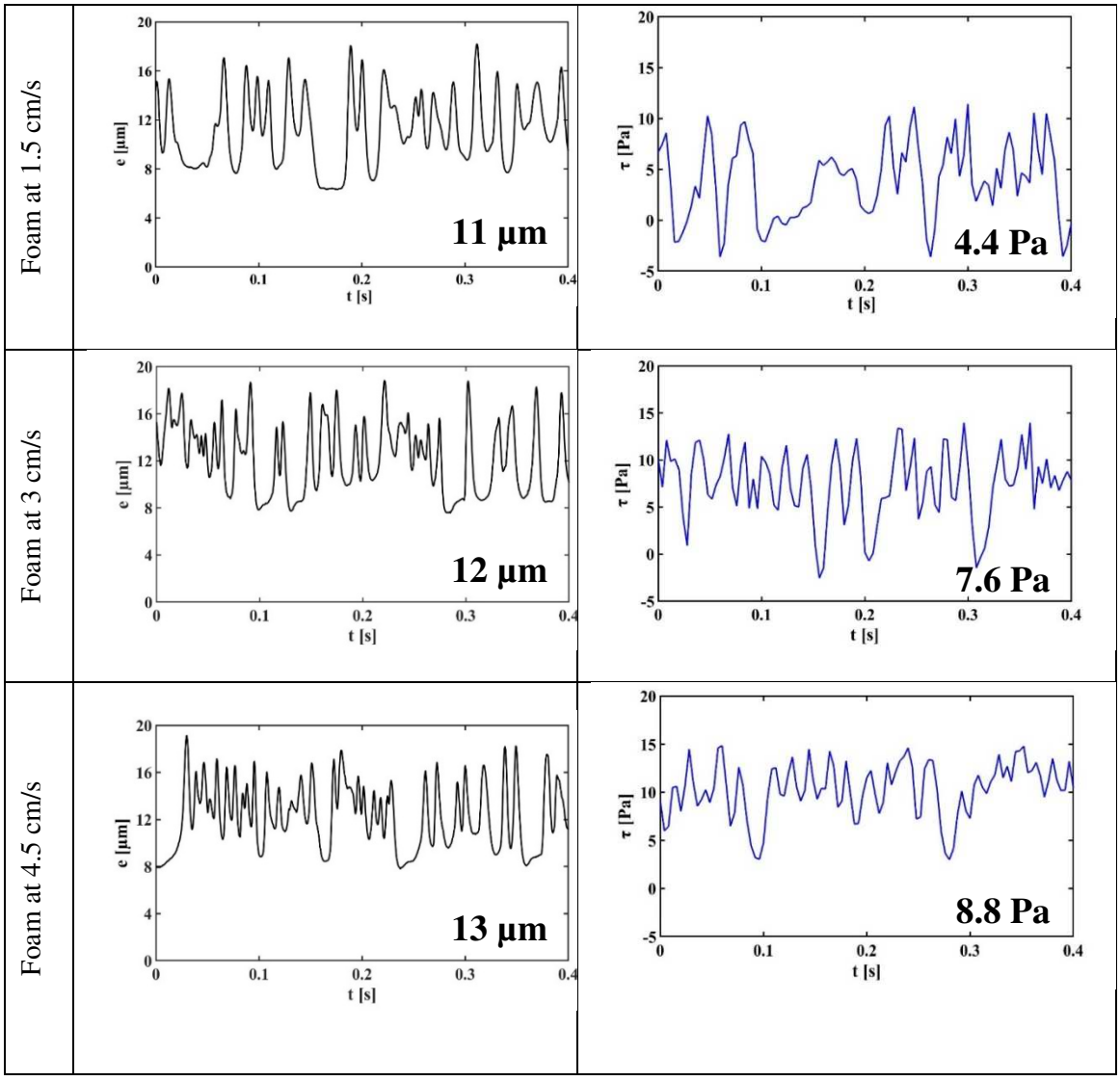

Fig. 4. Example of the evolution of wall film thickness (left) and wall shear stress (right) given by the temporal signals of conductimetry and polarography over the top wall for the three cases, respectively. The values indicated in the images show the mean thickness and the mean wall shear stress during 40 seconds of acquisition.

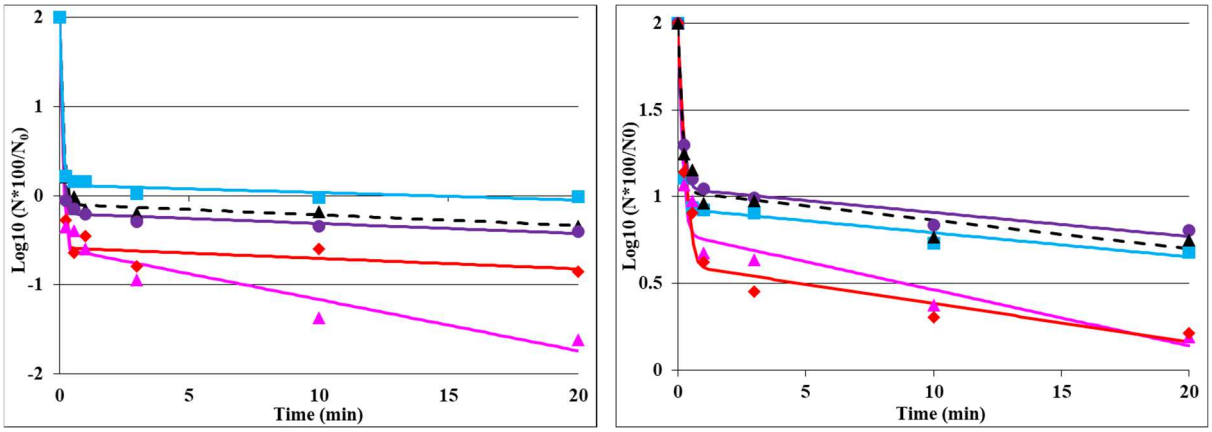

Fig. 5. Removal kinetics of *B. subtilis* PY79 (left) and *B. subtilis* PY79 *spsA* spores under the different flow conditions. Markers showed the data of three repetitions, and the line represents the biphasic fitted model fit to each condition: 1.5 cm/s (sky square), 4.5 cm/s (purple circle), 9 cm/s (pink triangle), 13.5 cm/s (red diamond), and CIP (black triangle).

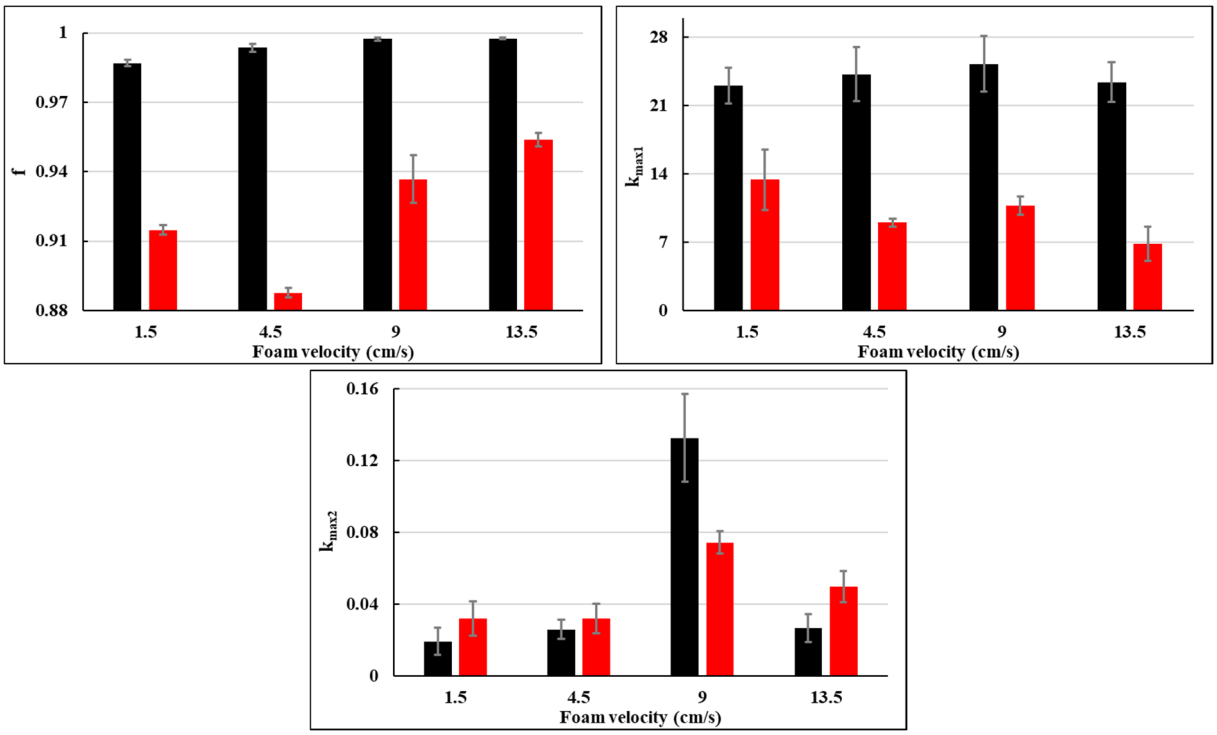

Fig. 6. kinetics parameters f, $K_{max1,}$ and K_{max2} for Bs PY79 (black color) and Bs PY79 *spsA* (red color) spores under different flow conditions.

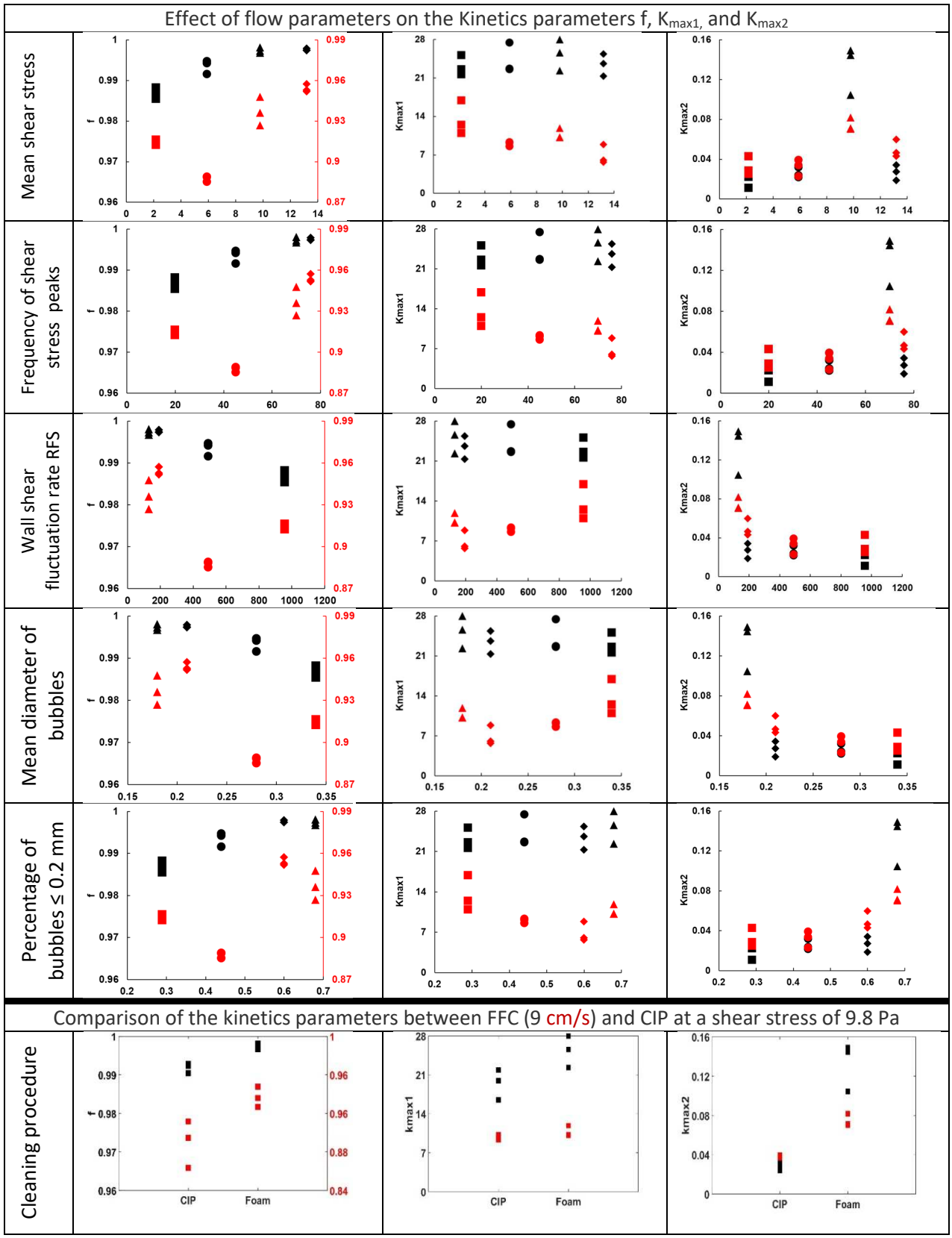

Fig. 7: Variations induced on the kinetics parameters f, K_{max1} and K_{max2} for Bs PY79 (black color) and Bs PY79 *spsA* (red color) spores under different flow conditions: 1.5 cm/s (square), 4.5 cm/s (circle), 9 cm/s (triangle), 13.5 cm/s (diamond), and CIP.

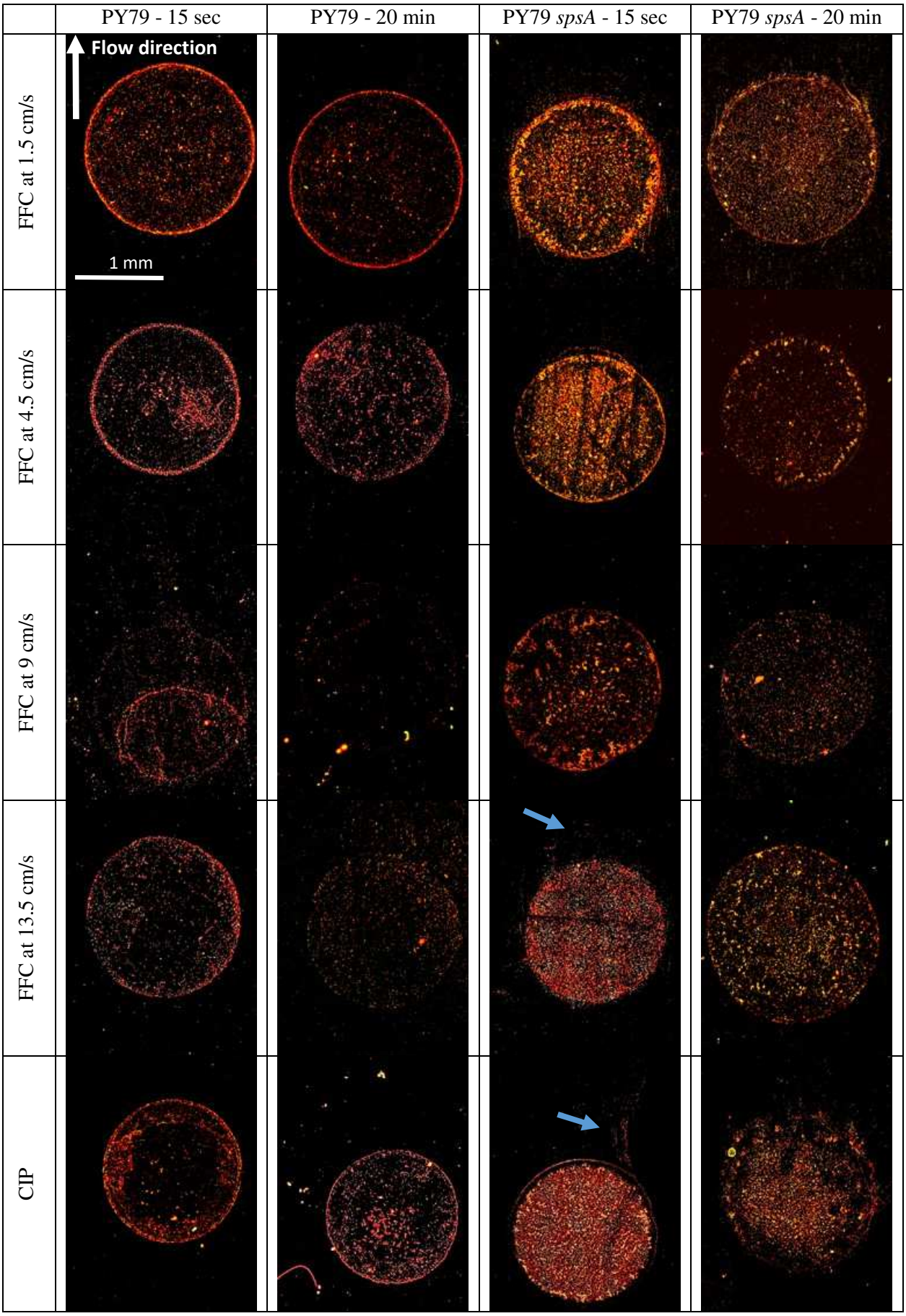
PY79 - 15 sec
PY79 - 20 min
PY79 spsA - 15 sec
PY79 spsA - 20 min
FFC at 1.5 cm/s
FFC at 4.5 cm/s
FFC at 9 cm/s
FFC at 13.5 cm/s
CIP
Flow direction
1 mm

Fig. 8: Residual deposition patterns of droplet contaminated with Bs spores after complete evaporation and further subjected to 5 seconds and 20 minutes of FFC and CIP procedures, examined by epifluorescence with a Zeiss Axioskop 2 plus microscope (x50). Blue arrows indicated the sliding of the spores observed at 15 s for Bs PY79 *spsA.*

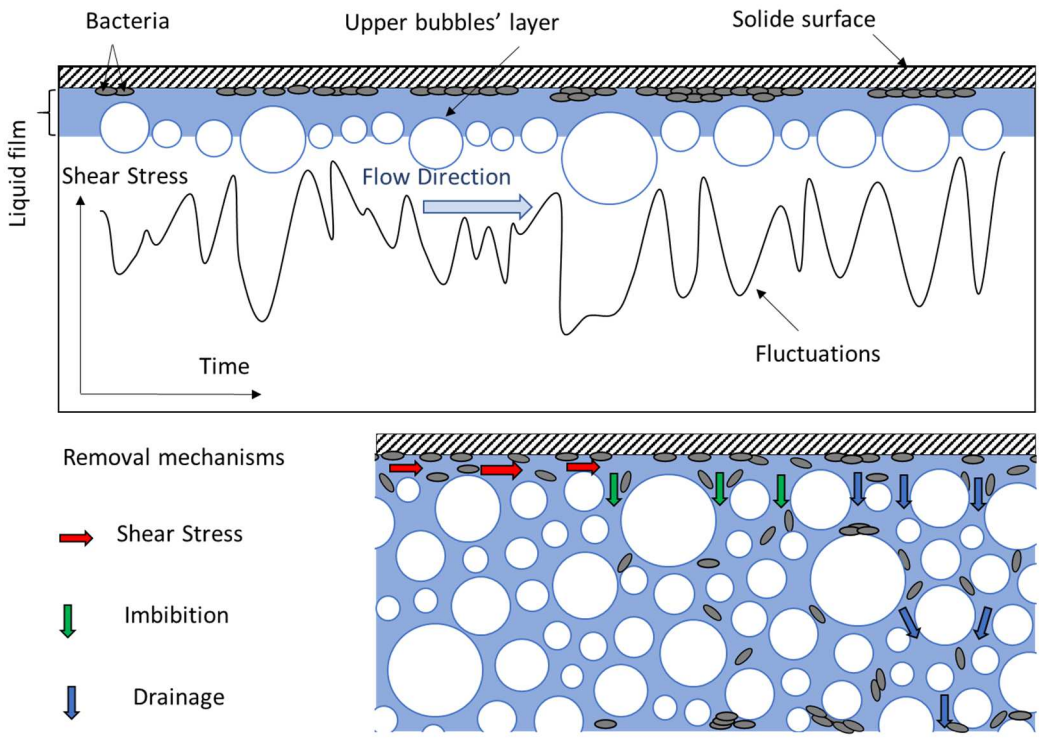

Fig. 9: Schematic of the suggested cleaning mechanisms using foam flow

Table 1: Description of the different flow conditions carried out. The FFC and CIP represent the foam flow conditions and the cleaning-in-place that has been processed for removal of Bacillus spores from stainless steel surfaces, respectively.

Flow conditions	**u (cm.s^{-1})**	**Ca [10^{-3}]**	**τ (Pa)**	**Dmean (mm)**	**F005**	**F02**	**RFS (%)**	**f (Hz)**
FFC	1.5	0. 5	2.2	0.34	0.002	0.29	957	20
	3	1.1	4.2	0.30	0.006	0.36	688	39
	4.5	1.6	5.9	0.28	0.013	0.44	491	45
	9	3.3	9.8	0.18	0.022	0.68	130	70
	13.5	4.8	13.2	0.21	0.043	0.60	193	76
CIP	180	----	10	----------				

Table 2: Tukey grouping for PY79 and *spsA* spores. According to the Tukey grouping, letters were indicated with potentially three classes A, AB, B, C and D depending on the parameter: common letters meaning no significant differences.

Mean Velocity of FFC conditions	f		Kmax1		Kmax2	
	PY79	*spsA*	PY79	*spsA*	PY79	*spsA*
1.5 cm/s	C	C	A	A	B	B
4.5 cm/s	B	D	A	AB	B	B
9 cm/s	A	B	A	AB	A	A
13.5 cm/s	A	A	A	B	B	B